Single-Walled Carbon Nanotube-Induced Lyotropic Phase Behavior of a Polymeric System

ARTICLE *in* MACROMOLECULES · DECEMBER 2012

Impact Factor: 5.8 · DOI: 10.1021/ma2021166

4 AUTHORS, INCLUDING:

Changwoo Do
Oak Ridge National Laboratory
48 PUBLICATIONS **277** CITATIONS
SEE PROFILE

Tae-Hwan Kim
Korea Atomic Energy Research Institute (KAERI)
31 PUBLICATIONS **239** CITATIONS
SEE PROFILE

Macromolecules

Article

pubs.acs.org/Macromolecules

Single-Walled Carbon Nanotube-Induced Lyotropic Phase Behavior of a Polymeric System

Hyung-Sik Jang,[†] Changwoo Do,[†] Tae-Hwan Kim,[†,‡] and Sung-Min Choi*,[†]

[†]Department of Nuclear and Quantum Engineering, Korea Advanced Institute of Science and Technology, Daejeon 305-701, Republic of Korea

[‡]Neutron Science Division, Department of Reactor Utilization and Development, Korea Atomic Energy Research Institute, Daejeon 305-353, Republic of Korea

Supporting Information

ABSTRACT: We report for the first time a new single-walled carbon nanotube (SWNT)-induced lyotropic phase behavior of a F108 block copolymer/water system. As the concentration is increased by evaporation, the F108-SWNT/water system exhibits isotropic−hexagonal−FCC−BCC−lamellar transitions. This is in clear contrast with the F108/water system (isotropic−BCC−lamellar transitions), indicating that the hexagonal and the FCC phases are newly induced by the presence of one-dimensional SWNTs. The SWNTs maintain their individuality or very small bundle state in all the phases except the lamellar phase. In the hexagonal phase, the SWNTs are located in the hydrophobic core of F108 cylinders oriented parallel to the [001] direction. The epitaxial transitions between the phases allowed us to identify the possible orientation of SWNTs in each phase: [110] in the FCC and either ⟨100⟩ or ⟨111⟩ in the BCC. In the lamellar phase, the SWNTs exist most likely in the hydrophobic layers forming aggregations among them. This new SWNT-induced lyotropic phase behavior in a block copolymer system may provide a new scalable route to fabricate SWNT superstructures with well-defined architecture and new functionalities.

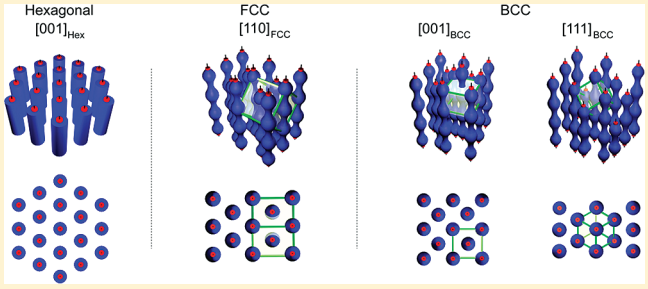

INTRODUCTION

For many practical applications of single-walled carbon nanotubes (SWNTs),[1] the fabrication of SWNT superstructures with well-defined morphology, density, and direction are highly required to enhance the physical properties of SWNTs collectively or to make new functionalities. Although many efforts have been made for this purpose using methods such as solvent evaporation,[2,3] electric,[4,5] magnetic,[6,7] or flow field,[8−11] an easy and simple method is yet to be developed. Amphiphilic molecules, such as block copolymers, exhibit rich phase behavior and have been extensively used as excellent templates for nanostructured materials.[12−14] Recently, there have been many efforts to incorporate nanoparticles,[15] such as spherical gold nanoparticles,[16,17] CdS nanoparticles,[18] and CdSe nanoparticles,[14] into self-assembled block copolymers to efficiently fabricate patterned nanoparticle−polymer composites. Theoretical studies and computer simulations predict that the cooperative self-assembly of functionalized nanoparticles and block copolymers can provide a wide variety of nanoparticle−polymer composites with well-controlled particle arrangements.[19−21] It is, therefore, highly desirable to use the rich phase behavior of block copolymers to fabricate well-controlled SWNT superstructures, which may provide an easy and scalable fabrication method. However, this approach is in its very early stage,[22,23] and to make this approach successful, it is essential to understand the phase behavior of polymeric systems when SWNTs are incorporated into the systems, which is the key information to design self-assembled SWNT superstructures using polymeric systems.

Here, we report a SWNT-induced lyotropic phase behavior in a Pluronic block copolymer system, which exhibits isotropic, hexagonal, face-centered cubic (FCC), body-centered cubic (BCC), and lamellar phases as concentration is increased. It should be noted that the hexagonal and FCC phases, which were not present in the block copolymer system, are newly induced by the presence of SWNTs. The expected location and orientation of SWNTs (which maintain their individuality or very small bundle state without aggregations) within the ordered phases are identified utilizing the epitaxial transitions between the phases.

EXPERIMENTAL SECTION

Materials. Purified HiPCO SWNTs (high-pressure CO conversion type, purity >90 wt %) were purchased from Unidym. Pluronic F108 (poly(ethylene oxide)$_{130}$−poly(propylene oxide)$_{60}$−poly(ethylene oxide)$_{130}$, PEO$_{130}$−PPO$_{60}$−PEO$_{130}$) was kindly provided by BASF Corporation and used without further purification. D_2O (99.9 mol % deuterium enriched) was purchased from Cambridge Isotope

Received: September 18, 2011
Revised: November 3, 2011
Published: December 22, 2011

Laboratory. H_2O was purified with a Millipore Direct Q system (electrical resistivity 18.2 MΩ cm) immediately before use.

Dispersion of SWNT and Sample Preparation. SWNTs of 0.09 g were added into 3 wt % Pluronic F108 in D_2O (0.9 g/30 g). To make the exfoliated SWNTs (individually isolated or very small bundles) adsorbed with Pluronic F108 (F108-SWNT), the mixtures were ultrasonicated for 1 h, followed by ultracentrifugation (ca. 110000*g*) for 4 h. After centrifugation, the upper ca. 70% of the dispersion was decanted to remove large bundled SWNTs at the bottom and freeze-dried. To prepare 5 wt % samples, the freeze-dried F108-SWNT powders were redispersed in distilled H_2O by mild shaking. This stock solution of F108-SWNT was divided into 20 tubes which were evaporated into different concentrations (5−100 wt % in 5 wt % steps). The F108 in H_2O samples at different concentration were prepared by the same manner, i.e., by evaporating 5 wt % samples of F108 in H_2O.

UV−vis−NIR Spectra. All the UV−vis−NIR spectra were measured by using a PerkinElmer L-750 UV−vis−NIR spectrometer. For the F108-SWNT samples with low viscosity, standard quartz cells of 2 mm beam path length were used, and for the F108-SWNT samples with high viscosity, two quartz plates (between which samples were placed) were used.

Small-Angle Neutron Scattering Measurements. Small-angle neutron scattering (SANS) measurements were performed using the 40 m SANS instrument at the HANARO, the Korea Atomic Energy Research Institute (KAERI) in Daejeon, Republic of Korea. Neutrons of wavelength λ = 6 Å with a full width half-maximum $\Delta\lambda/\lambda$ = 12% were used. Three configurations of sample-to-detector distance of 1.16, 7.78, and 17.9 m were used to cover the q range of 0.003 $Å^{-1} < q < 0.6$ $Å^{-1}$, where $q = (4\pi/\lambda)\sin(\theta/2)$ is the magnitude of the scattering vector and θ is the scattering angle. Sample scattering was corrected for background and empty cell scattering and the sensitivity of individual detector pixels. The corrected data sets were placed on an absolute scale through the secondary standard method. All the SANS measurements were carried out at 25 °C using quartz cells of 2 mm path length.

Atomic Force Microscopy Measurement. Atomic force microscopy (AFM) images were taken in tapping mode by using a VEECO AFM instrument (Digital Instrument). For the AFM measurements, the as-prepared F108-SWNT dispersion was spin-coated (at 4000 rpm for 2 min) onto silicon wafers. To prepare the samples for bare SWNTs, the F108-SWNT dispersion deposited onto a silicon wafer was burned at 650 °C for 6 h in an argon atmosphere to remove the Pluronic F108 adsorbed on SWNTs.

Small-Angle X-ray Scattering Measurements. Small-angle X-ray scattering (SAXS) measurements were performed on the 4C1 beamline at Pohang Accelerator Laboratory (PAL), Republic of Korea, where a W/B4C double multilayer monochromator delivered monochromatic X-rays with a wavelength of 0.1608 nm and a wavelength spread $\Delta\lambda/\lambda$ of 0.01. A two-dimentional CCD camera (Mar CCD, Mar USA, Inc., CCD165) was used to collect scattered X-rays. Sample cells with a path length of 0.8 mm enclosed by two thin Kapton windows were used. The sample-to-detector distance was 1 m, covering the q range of 0.2 $nm^{-1} < q < 3.2$ nm^{-1}. The q values were calibrated using silver behenate ($AgO_2C(CH_2)_{20}CH_3$). All measurements were performed at room temperature.

RESULTS AND DISCUSSION

Pluronic F108 (PEO_{130}−PPO_{60}−PEO_{130}) is a triblock copolymer which shows various phases in water depending on concentration at room temperature.[24,25] The F108-SWNT was prepared by sonicating the mixture of SWNTs and F108 in water for 1 h, followed by ultracentrifugation and freeze-drying of supernatant. To enhance the ultracentrifugation efficiency, D_2O was used. The decanted dispersion was stable for more than 2 months without any precipitation (Figure 1a). The UV−vis−NIR spectrum of as-prepared F108-SWNT dispersion shows sharp van Hove transition peaks (Figure 1b), indicating

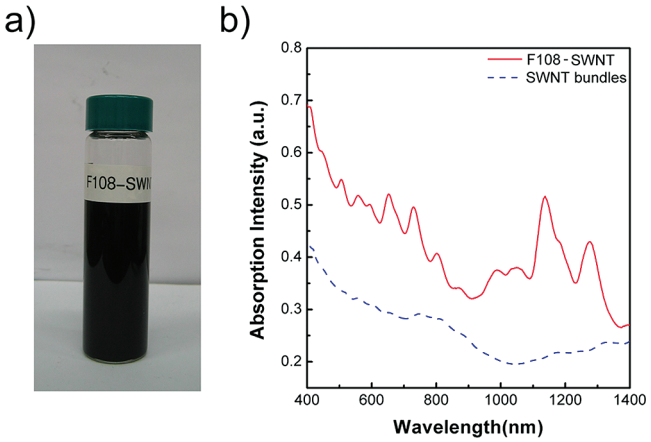

Figure 1. (a) F108-SWNT dispersion after ultracentrifugation. (b) UV−vis−NIR spectra of F108-SWNT dispersed in water and bundled SWNTs.

that SWNTs exist in an isolated form or in a very small bundle. The concentrations of SWNT and F108 in the decanted solution determined by using Beer's law,[26,27] and the dried mass of the decanted dispersion is 0.011 and 2.1 wt %, respectively.

To further characterize the dispersion quality of the decanted F108-SWNT in D_2O, the SANS measurements were performed at 25 °C using the 40 m SANS instrument at the HANARO neutron facility, Korea Atomic Energy Research Institute (KAERI), Korea. As a comparison, an F108 only sample in D_2O prepared at the same concentration as that of the decanted dispersion was also measured. The SANS intensities are shown in Figure 2. Since F108 at 2.1 wt % in water does not

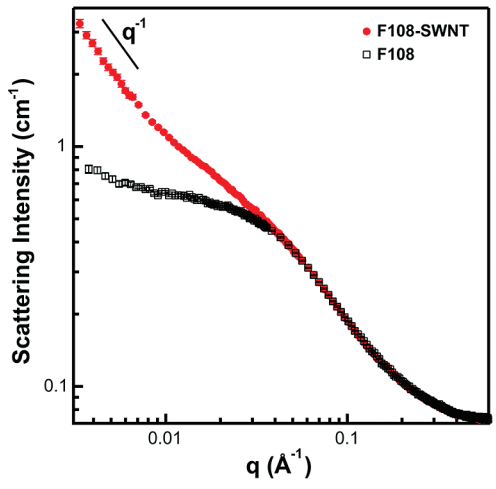

Figure 2. SANS intensities of as-prepared F108-SWNT and F108 only in D_2O at 25 °C. The concentration of both samples was 2.1 wt %.

make micelles at 25 °C (Supporting Information), the scattering intensity of F108 only shows a pattern typical for fully dissolved Gaussian polymer chains in the solution.[28,29] On the other hand, the scattering intensity of F108-SWNT in D_2O shows at a clear q^{-1} behavior in the low-q region (where $q = (4\pi/\lambda)\sin(\theta/2)$ is the magnitude of scattering vector, λ is neutron wavelength, and θ is scattering angle), which is typical for long, thin, cylindrical nanoparticles dispersed in solu-

dx.doi.org/10.1021/ma2021166 | Macromolecules 2012, 45, 986−992

tion.[30,31] This clearly indicates that SWNTs are well dispersed without forming aggregations or networks.

The diameter and length distribution of bare SWNTs (obtained by burning F108-SWNT on silicon wafer in Ar atmosphere) were determined from the AFM measurements (Figure 3).[30,32] The diameter distribution of bare SWNTs is

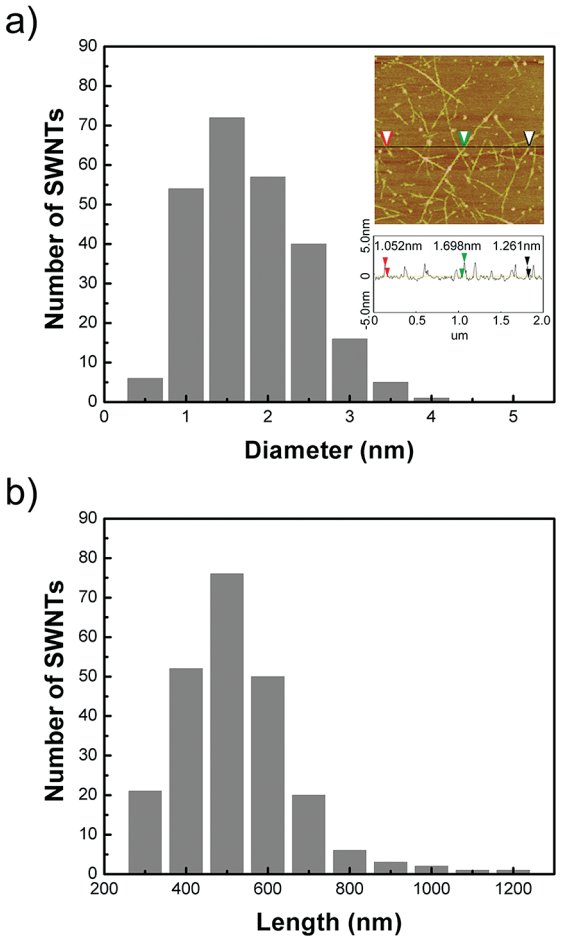

Figure 3. (a) Diameter and (b) length distributions of bare SWNTs after burning F108-SWNTs at 650 °C for 6 h in an Ar atmosphere. The inset shows a representative AFM image.

peaked at 1.5 ± 0.25 nm, and the diameter less than 2.5 nm occupies 84% of the distribution, which indicates that F108-SWNT are dispersed in an isolated form or in a very small bundle. The length distribution is peaked at 500 ± 50 nm with a mean length of ca. 500 nm.

The F108-SWNT samples in H_2O with different concentrations (5−100 wt % in 5 wt % steps) were prepared by evaporating 5 wt % samples (which were prepared by redispersing freeze-dried F108-SWNT in H_2O by mild shaking). The UV−vis−NIR spectra of F108-SWNT at various concentrations (up to 70 wt %) show sharp van Hove transition peaks which are essentially identical with that of as-prepared F108-SWNT dispersion (Figure 4). This clearly indicates that the exfoliated SWNTs are well maintained even at high concentrations without aggregations. However, when the concentration is 80 wt % or higher, the sharp peaks becomes flattened, indicating aggregation of SWNTs. This is directly related with the lamellar phase of F108 which appears at 80 wt %. This will be discussed more in detail later.

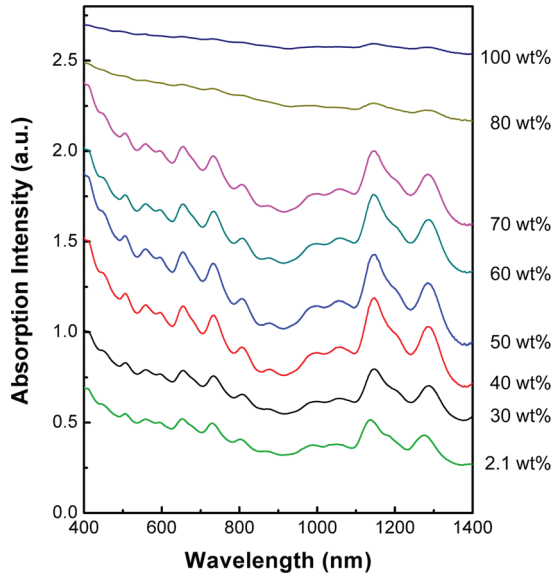

Figure 4. UV−vis−NIR spectra of F108-SWNT in water at different concentration. The spectra are shifted vertically for visual clarity.

To characterize the difference in phase behavior depending on the existence of SWNTs, SAXS measurements of F108 only and F108-SWNT dispersions at different concentrations were performed at room temperature using the 4C1 beamline at the Pohang Accelerator Laboratory, Korea. The SAXS intensities of F108 only and F108-SWNT in water at different concentrations are shown in Figure 5. The SAXS intensities show that the F108 only in water (without SWNTs) goes through isotropic, BCC, and lamellar phases as the concentration is increased. At 5 wt %, F108 polymers are fully dissolved and micelles are not formed. As the concentration is increased, the F108 only forms isotropic micellar phase as shown by the SAXS intensity at 15 wt %. At 25 wt %, the SAXS intensity shows a broad peak near 0.67 nm^{-1}, indicating that F108 solution starts to form an ordered structure. In the concentration range from 30 to 65 wt %, the SAXS intensities show sharp peaks with the peak position ratio of $1:\sqrt{2}:\sqrt{3}:\sqrt{4}:\sqrt{5}:\sqrt{6}:\sqrt{7}$, indicating the BCC phase. At 70 and 75 wt %, the SAXS intensities show peaks relevant to BCC and lamellar structures, indicating a mixed phase. When the concentration is higher than 80 wt %, the F108 solution forms a lamellar phase as indicated by the peak position ratio of 1:2:3.

The SAXS intensities of F108-SWNT samples show a sequence of changes with concentration, which is clearly different from that of F108 only samples. The SAXS intensities of F108-SWNT samples at 5 and 15 wt % show an upturn in the low-q region which is induced by the presence of long and thin SWNTs. This scattering pattern is clearly different from that of the isotropic spherical micellar phase which was observed in the F108 only sample at 15 wt %. When the concentration is increased to 20 wt %, a few small peaks start to build up (not shown), and at 25 wt %, a scattering pattern with a peak position ratio of $1:\sqrt{3}:\sqrt{4}:\sqrt{7}:\sqrt{9}:\sqrt{12}$ (with a lattice parameter of 23.8 nm) becomes apparent, indicating the formation of hexagonal phase. This scattering pattern is maintained up to 30 wt %. It should be noted that the hexagonal phase was not observed in the F108 only samples at any concentration. It is clear, therefore, that the hexagonal phase is induced by the long one-dimensional shape of SWNTs (adsorbed by F108), forming hexagonal arrays of SWNTs

dx.doi.org/10.1021/ma2021166 | Macromolecules 2012, 45, 986−992

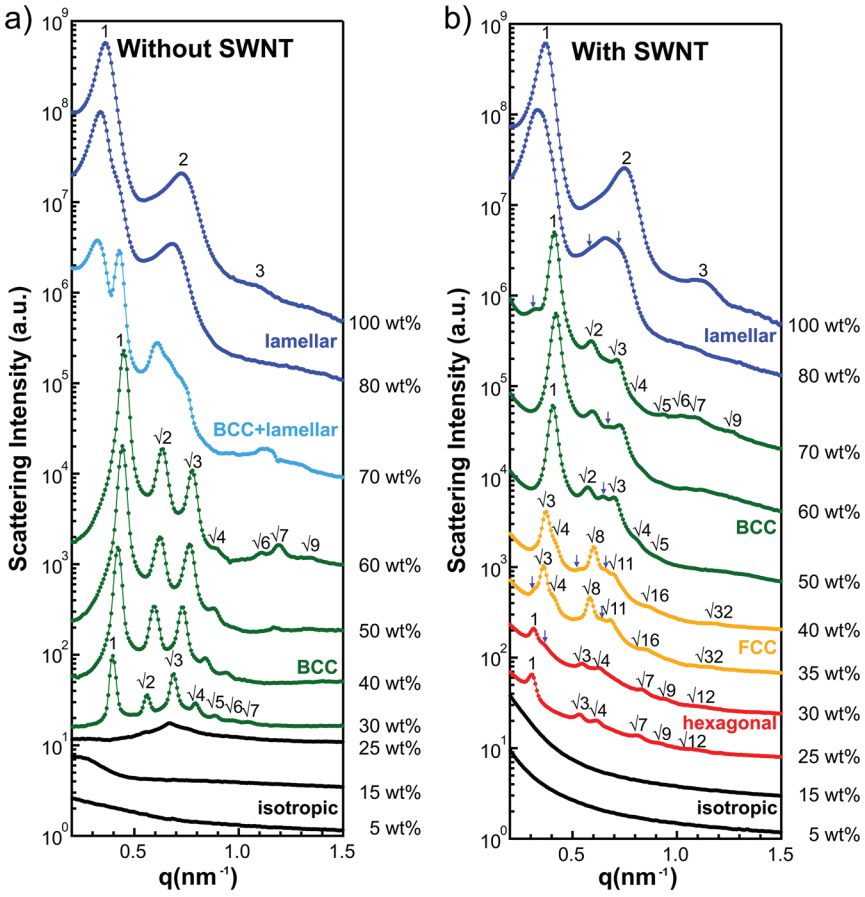

Figure 5. SAXS intensities of (a) F108 and (b) F108-SWNT in H_2O at different concentration at room temperature. The relative peak position ratios relevant to each phase are presented. The peaks indicated by arrows show some mixture of phases. Scattering intensities are shifted vertically for visual clarity. The peak positions (except those indicated by arrows) of each scattering pattern are given in the Supporting Information, Tables S1 and S2.

which are centered at the cylindrical hydrophobic core of F108. It should be noted that no other peaks, which do not correspond to the hexagonal phase, were observed in the scattering intensity of the 25 wt % sample. This indicates that the hexagonal phase at 25 wt % is homogeneous without forming any phase separation or a mixed phase. This may indicate that majority of F108 are adsorbed on the surface of SWNTs. When the concentration is increased to 35 wt %, the F108-SWNT system makes a topological transition to the FCC phase, as indicated by the peak position ratio of $\sqrt{3}:\sqrt{4}:\sqrt{8}:\sqrt{11}:\sqrt{16}:\sqrt{32}$. The FCC phase is maintained up to 40 wt %. It should be also noted that the FCC phase was not observed in the F108 only samples at any concentrations measured in this study. Therefore, it is clear that the FCC phase is induced by the existence of SWNTs, although the physical mechanism for the formation of FCC phase in the F108-SWNT solution is not clear. As the concentration is increased to 45 wt %, the SAXS intensity shows a mixed phase of the FCC and the BCC. At 50 wt %, the BCC peaks become dominant with a peak position ratio of $1:\sqrt{2}:\sqrt{3}:\sqrt{4}:\sqrt{5}:\sqrt{6}:\sqrt{7}$. The BCC phase is maintained up to 75 wt %. The SAXS intensities at 80 wt % or higher show that the F108-SWNT systems finally transform into the lamellar phase as it was seen in the F108 only samples.

Summarizing the phase behaviors, the F108-SWNT system makes a sequence of phase transitions, isotropic−hexagonal−FCC−BCC−lamellar phases, as the concentration is increased from 5 to 100 wt %, which is in clear contrast with the sequence of phase transitions of the F108 only system, isotropic−BCC−lamellar phases. The hexagonal and FCC phases are newly induced by the presence of SWNTs. It should be noted that while the hexagonal phase in polymeric systems is typically observed between the cubic and lamellar phases, the hexagonal phase in the F108-SWNT system was observed before the cubic phase due to the presence of long one-dimensional objects, SWNTs. To the best of our knowledge, this is the first observation of hexagonal phase in polymeric system induced by SWNTs.

The lattice parameter of each phase was calculated from the first-order Bragg peaks q_1 using $a_{hex} = 4\pi/\sqrt{3}q_1$ for the hexagonal, $a_{fcc} = \sqrt{3}\cdot 2\pi/q_1$ for the FCC, $a_{bcc} = \sqrt{2}\cdot 2\pi/q_1$ for the BCC, and $a_{lam} = 2\pi/q_1$ for the lamellar phase. The results are summarized in Figure 6. While the SAXS intensities show some signatures of mixed phases (as indicated by arrows in Figure 5), for simplicity, only the dominant phases are presented, except the cases where the weightings of two constituting phases are similar.

Since F108 works as a dispersion agent of SWNTs in water (with its hydrophobic PPO segment adsorbed on the surface of SWNT and its hydrophilic PEO segments facing water[33−35]), it is naturally expected that the SWNTs in the hexagonal phase are located at the center of cylindrical hydrophobic core of F108 with their long axes oriented along the [001] direction. Since the hexagonal phase is transformed into the FCC phase

dx.doi.org/10.1021/ma2021166 | *Macromolecules* 2012, 45, 986−992

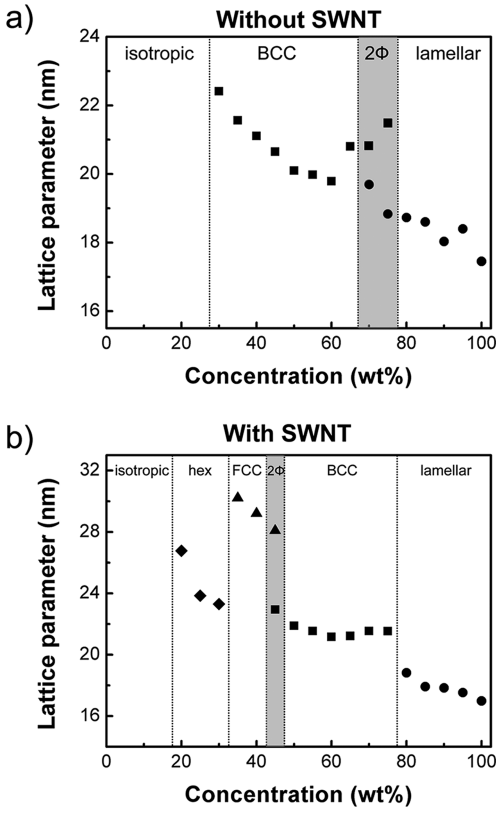

Figure 6. Lattice parameter of (a) F108 and (b) F108-SWNT in water at different concentration corresponding to each phase.

with the dispersion quality of SWNTs fully maintained (as clearly indicated by the UV−vis−NIR spectra in Figure 4), it is also expected that spherelike micelles of F108 are formed on SWNTs with the hydrophobic cores of the micelles pierced through by the SWNTs. If this is not the case, the good dispersion quality of SWNTs as shown by the UV−vis−NIR spectra cannot be maintained. Similar structures are expected for the BCC phase as well. In the lamellar phase, the SWNTs should be present in the PPO domains. While the PPO domains of the FCC and BCC phases are enclosed by the PEO domains (maintaining the isolation of SWNTs), the PPO domains of the lamellar phase are fully open in the transverse direction. Therefore, the SWNTs in each two-dimensional PPO domain can aggregate easily. In fact, this should be the reason why the UV−vis−NIR spectra at 80 wt % or higher concentration are flattened.

Since all the samples that formed the FCC and the BCC phases were prepared by evaporating 5 wt % samples, they went through the hexagonal phase at which the SWNTs are oriented along the [001] direction (Figure 7a). Therefore, it is expected that there should be a preferred direction of SWNTs in the FCC and the BCC phase. Recently, it was shown that the hexagonal to FCC phase transition in block copolymer solution occurs epitaxially and the cylindrical axis (the [001] direction of hexagonal phase) coincides with the [110] direction of FCC structure.[36] Therefore, it is expected that the SWNTs in the FCC phase are oriented along the [110] direction (Figure 7b). The FCC to BCC transition in block copolymer solution is also epitaxial and commonly described by the well-known Bain distortion in which a distorted BCC unit cell imbedded in two FCC unit cells transforms to a BCC unit cell by compressing along one ⟨100⟩ direction and expanding along two ⟨110⟩ directions of the FCC unit cell. In this FCC to BCC transition, the {111} planes of the FCC structure are parallel with the {110} planes of the BCC structure[37,38] and the [110] direction of FCC structure coincides with either the ⟨100⟩ or ⟨111⟩ direction of BCC structure. Therefore, it is expected that the SWNTs in the BCC phase are oriented along the ⟨100⟩ or ⟨111⟩ direction (Figure 7c). Finally, the {110} planes in the BCC phase, where the areal number density of micelle is the highest and both of ⟨100⟩ and ⟨111⟩ vectors are present, are expected to form the hydrophobic layers of lamellar structure, resulting in the aggregation of SWNTs possibly with a preferred orientation parallel to their orientation in the BCC phase.

To support the epitaxial phase transitions in the F108-SWNT system which we used to identify the orientations of SWNTs in the ordered phases, the areal number densities of SWNTs at the hexagonal, FCC, and BCC phases are calculated using the measured lattice parameters. Here, the areal number density of SWNTs is defined as the number of SWNTs per unit area in the plane perpendicular to the orientation of SWNTs. In this calculation, it was assumed that all the hydrophobic cores of cylinders in the hexagonal phases are filled with SWNTs and all the spherelike micelles in the FCC and BCC phases are pierced through by SWNTs. If the F108-SWNT system makes epitaxial transitions as described above, the areal number density of SWNTs should change smoothly across the phase

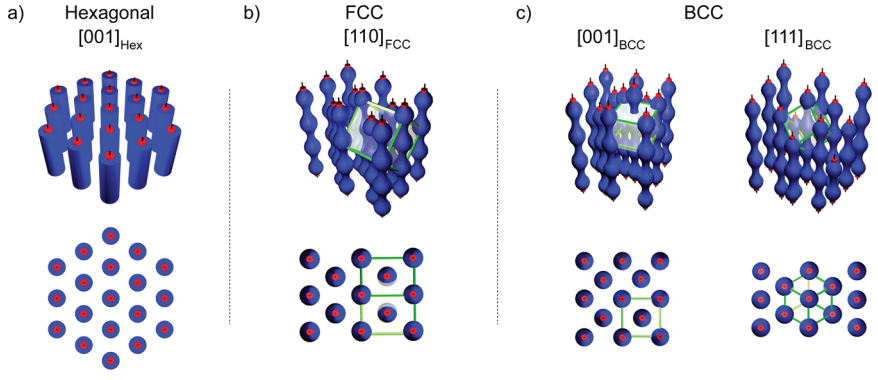

Figure 7. Schematics for the structures of F108-SWNT in water at different phases: (a) hexagonal, (b) FCC, and (c) BCC phases. The boxes in green color represent unit cells. The orientation of SWNTs in each phase is specified in each figure and the views from the directions of SWNTs are given on the bottom side of each figure. Here, for the BCC phase, [001] and [111] directions were used as representative directions for ⟨100⟩ and ⟨111⟩, respectively. Colors represent PPO (red), PEO (blue), and SWNT (black).

dx.doi.org/10.1021/ma2021166 | *Macromolecules* 2012, 45, 986−992

transitions. Also, since all the samples were prepared by evaporating 5 wt % samples, the areal number density of SWNTs should increases smoothly with concentration. The areal number densities of SWNTs, which were calculated for the SWNTs orientations identified based on the epitaxial transitions (the [001] direction in the hexagonal phase, the [110] direction in the FCC phase, and either the ⟨100⟩ or ⟨111⟩ direction in the BCC phase), change smoothly across the phase transitions (Figure 8). For all other orientations, the areal

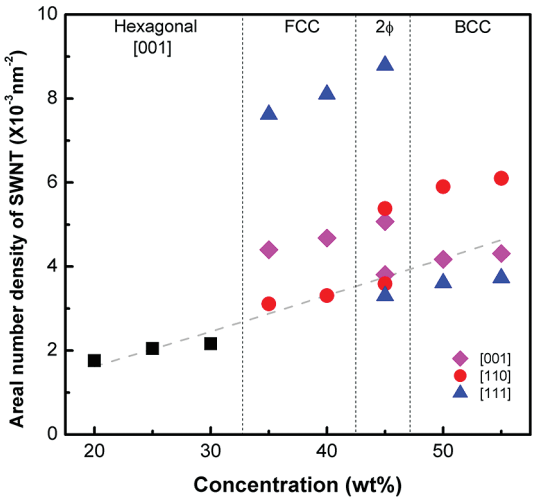

Figure 8. Areal number density of SWNTs at different concentrations calculated using the measured lattice parameters. The dotted line is a guide for eyes, showing that the areal number density of SWNTs changes smoothly across the phase transitions when the directions of SWNTs are [001] in hexagonal, [110] in FCC, and either ⟨100⟩ or ⟨111⟩ in BCC phases. Here, for the BCC phase, [001] and [111] directions were used as representative directions for ⟨100⟩ and ⟨111⟩, respectively.

number density of SWNTs clearly deviates from the smooth linear change across the phase transitions. This results support the epitaxial transitions in the F108-SWNT system from which the directions of SWNTs in the FCC and BCC phases are identified.

CONCLUSION

We report for the first time a new SWNT-induced lyotropic phase behavior of Pluronic F108 block copolymer system. As the concentration increases from 5 to 100 wt %, the F108-SWNT in water exhibit a sequence of phase transitions, isotropic−hexagonal−FCC−BCC−lamellar transitions, which is in clear contrast with that of the F108 only samples, isotropic−BCC−lamellar transitions. This clearly indicates that the hexagonal and the FCC phases are newly induced by the presence of long one-dimensional SWNTs. The SWNTs maintain their individuality or very small bundle state up to 80 wt % before the lamellar phase is formed. These suggest that, in the hexagonal phase, the SWNTs are located in the hydrophobic core of F108 cylinders. The epitaxial transitions between the hexagonal and the FCC phases and between the FCC and the BCC phases allowed us to identify the possible orientations of SWNTs in the FCC and the BCC phases: [110] in the FCC and either ⟨100⟩ or ⟨111⟩ in the BCC. In the lamellar phase, the SWNTs exist most likely in the hydrophobic layers, forming aggregations among them. This new SWNT-induced lyotropic phase behavior in a block copolymer system may provide a new scalable route to fabricate SWNT superstructures with well-defined architecture and new functionalities. Furthermore, this may provide new possibilities for self-assembling other one-dimensional nanoparticles into highly ordered superstructures using the phase behavior of block copolymer systems.

ASSOCIATED CONTENT

Supporting Information

Measurements of micellization of F108 in water and a summary of scattering peak positions of F108 and F108-SWNT in water. This material is available free of charge via the Internet at http://pubs.acs.org.

AUTHOR INFORMATION

Corresponding Author

*E-mail: sungmin@kaist.ac.kr.

ACKNOWLEDGMENTS

This work was supported by the National Research Foundation grants funded by the Ministry of Education, Science and Technology of the Korean government (Nos. 2011-0000383 and 2011-0018680) and a grant from the Construction Technology Innovation Program funded by the Ministry of Land, Transportation and Maritime Affairs of the Korean government. The authors acknowledge the Pohang Accelerator Laboratory for providing access to the beamline 4C1 and the HANARO Center of the Korea Atomic Energy Research Institute for providing access to the 40 m SANS instrument used in this work.

REFERENCES

(1) Baughman, R. H.; Zakhidov, A. A.; de Heer, W. A. *Science* **2002**, *297*, 787−792.
(2) Simmons, T. J.; Hashim, D.; Vajtai, R.; Ajayan, P. M. *J. Am. Chem. Soc.* **2007**, *129*, 10088−10089.
(3) Shimoda, H.; Oh, S. J.; Geng, H. Z.; Walker, R. J.; Zhang, X. B.; McNeil, L. E.; Zhou, O. *Adv. Mater.* **2002**, *14*, 899−901.
(4) Kamat, P. V.; Thomas, K. G.; Barazzouk, S.; Girishkumar, G.; Vinodgopal, K.; Meisel, D. *J. Am. Chem. Soc.* **2004**, *126*, 10757−10762.
(5) Park, C.; Wilkinson, J.; Banda, S.; Ounaies, Z.; Wise, K. E.; Sauti, G.; Lillehei, P. T.; Harrison, J. S. *J. Polym. Sci., Part B: Polym. Phys.* **2006**, *44*, 1751−1762.
(6) Tumpane, J.; Karousis, N.; Tagmatarchis, N.; Norden, B. *Angew. Chem., Int. Ed.* **2008**, *47*, 5148−5152.
(7) Sano, N.; Naito, M.; Kikuchi, T. *Carbon* **2007**, *45*, 78−82.
(8) Geblinger, N.; Ismach, A.; Joselevich, E. *Nature Nanotechnol.* **2008**, *3*, 195−200.
(9) Xin, H.; Woolley, A. T. *Nano Lett.* **2004**, *4*, 1481−1484.
(10) Huang, Y.; Duan, X.; Wei, Q.; Lieber, C. M. *Science* **2001**, *291*, 630−633.
(11) Lay, M. D.; Novak, J. P.; Snow, E. S. *Nano Lett.* **2004**, *4*, 603−606.
(12) Ruzette, A.-V.; Leibler, L. *Nature Mater.* **2005**, *4*, 19−31.
(13) Bates, F. S.; Fredrickson, G. H. *Phys. Today* **1999**, *52*, 32−38.
(14) Lin, Y.; Boker, A.; He, J.; Sill, K.; Xiang, H.; Abetz, C.; Li, X.; Wang, J.; Emrick, T.; Long, S.; Wang, Q.; Balazs, A.; Russell, T. P. *Nature* **2005**, *434*, 55−59.
(15) Vaia, R. A.; Maguire, J. F. *Chem. Mater.* **2007**, *19*, 2736−2751.
(16) Bockstaller, M. R.; Lapetnikov, Y.; Margel, S.; Thomas, E. L. *J. Am. Chem. Soc.* **2003**, *125*, 5276−5277.
(17) Chiu, J. J.; Kim, B. J.; Kramer, E. J.; Pine, D. J. *J. Am. Chem. Soc.* **2005**, *127*, 5036−5037.
(18) Yeh, S. W.; Wei, K. H.; Sun, Y. S.; Jeng, U. S.; Liang, K. S. *Macromolecules* **2005**, *38*, 6559−6565.

(19) Thompson, R. B.; Ginzburg, V. V.; Matsen, M. W.; Balazs, A. C. *Science* **2001**, *292*, 2469−2472.
(20) Kang, H.; Detcheverry, F. A.; Mangham, A. N.; Stoykovich, M. P.; Daoulas, K. C.; Hamers, R. J.; Muller, M.; de Pablo, J. J.; Nealey, P. F. *Phys. Rev. Lett.* **2008**, *100*, 148303.
(21) Sknepnek, R.; Anderson, J. A.; Lamm, M. H.; Schmalian, J.; Travesset, A. *ACS Nano* **2008**, *2*, 1259−1265.
(22) Doe, C.; Jang, H.-S.; Kim, T.-H.; Kline, S. R.; Choi, S.-M. *J. Am. Chem. Soc.* **2009**, *131*, 16568−16572.
(23) Doe, C.; Jang, H.-S.; Kline, S. R.; Choi, S.-M. *Macromolecules* **2010**, *43*, 5411−5416.
(24) Yardimci, H.; Chung, B.; Harden, J. L.; Leheny, R. L. *J. Chem. Phys.* **2005**, 123.
(25) Mohan, P. H.; Bandyopadhyay, R. *Phys. Rev. E* **2008**, *77*, 041803.
(26) Wenseleers, W.; Vlasov, I. I.; Goovaerts, E.; Obraztsova, E. D.; Lobach, A. S.; Bouwen, A. *Adv. Funct. Mater.* **2004**, *14*, 1105−1112.
(27) Matarredona, O.; Rhoads, H.; Li, Z.; Harwell, J. H.; Balzano, L.; Resasco, D. E. *J. Phys. Chem. B* **2003**, *107*, 13357−13367.
(28) Mortensen, K. *J. Phys.: Condens. Matter* **1996**, *8*, A103−A124.
(29) Jain, N. J.; Aswal, V. K.; Goyal, P. S.; Bahadur, P. *J. Phys. Chem. B* **1998**, *102*, 8452−8458.
(30) Kim, T.-H.; Doe, C.; Kline, S. R.; Choi, S.-M. *Adv. Mater.* **2007**, *19*, 929−933.
(31) Kim, T.-H.; Doe, C.; Kline, S. R.; Choi, S.-M. *Macromolecules* **2008**, *41*, 3261−3266.
(32) Islam, M. F.; Rojas, E.; Bergey, D. M.; Johnson, A. T.; Yodh, A. G. *Nano Lett.* **2003**, *3*, 269−273.
(33) Florent, M.; Shvartzman-Cohen, R.; Goldfarb, D.; Yerushalmi-Rozen, R. *Langmuir* **2008**, *24*, 3773−3779.
(34) Nativ-Roth, E.; Shvartzman-Cohen, R.; Bounioux, C.; Florent, M.; Zhang, D.; Szleifer, I.; Yerushalmi-Rozen, R. *Macromolecules* **2007**, *40*, 3676−3685.
(35) Shvartzman-Cohen, R.; Florent, M.; Goldfarb, D.; Szleifer, I.; Yerushalmi-Rozen, R. *Langmuir* **2008**, *24*, 4625−4632.
(36) Park, M. J.; Char, K.; Bang, J.; Lodge, T. P. *Langmuir* **2005**, *21*, 1403−1411.
(37) Bang, J.; Lodge, T. P.; Wang, X.; Brinker, K. L.; Burghardt, W. R. *Phys. Rev. Lett.* **2002**, *89*, 215505.
(38) Bang, J.; Lodge, T. P. *J. Phys. Chem. B* **2003**, *107*, 12071−12081.